JACS Au
AN OPEN ACCESS JOURNAL OF THE AMERICAN CHEMICAL SOCIETY

pubs.acs.org/jacsau

Article

Electrodetection of Small Molecules by Conformation-Mediated Signal Enhancement

Krishnan Murugappan,[¶] Uthayasuriya Sundaramoorthy,[¶] Adam M. Damry,[¶] David R. Nisbet, Colin J. Jackson,[*] and Antonio Tricoli[*]

Cite This: *JACS Au* 2022, 2, 2481−2490

Read Online

ACCESS | Metrics & More | Article Recommendations | Supporting Information

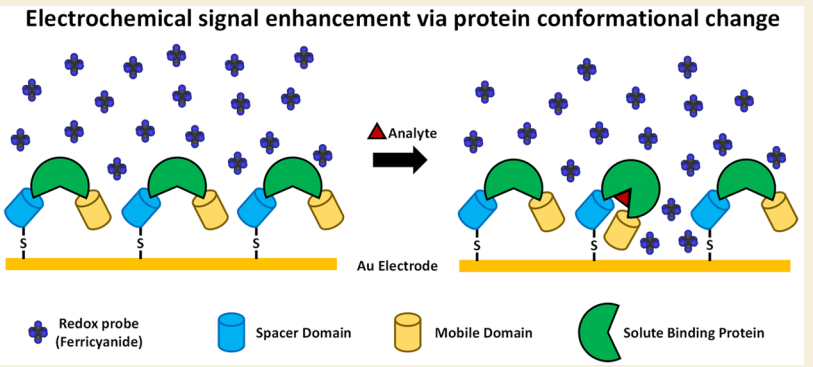

ABSTRACT: Electrochemical biosensors allow the rapid, selective, and sensitive transduction of critical biological parameters into measurable signals. However, current electrochemical biosensors often fail to selectively and sensitively detect small molecules because of their small size and low molecular complexity. We have developed an electrochemical biosensing platform that harnesses the analyte-dependent conformational change of highly selective solute-binding proteins to amplify the redox signal generated by analyte binding. Using this platform, we constructed and characterized two biosensors that can sense leucine and glycine, respectively. We show that these biosensors can selectively and sensitively detect their targets over a wide range of concentrations—up to 7 orders of magnitude—and that the selectivity of these sensors can be readily altered by switching the bioreceptor's binding domain. Our work represents a new paradigm for the design of a family of modular electrochemical biosensors, where access to electrode surfaces can be controlled by protein conformational changes.

KEYWORDS: *biosensing, electrochemistry, small molecule sensing, proteins, ligand binding, conformational change, differential pulse voltammetry*

INTRODUCTION

The ability to detect biomolecules rapidly, sensitively, and selectively with portable and small footprint devices is desirable because biomarker concentrations encode a wealth of information regarding metabolic function and health, which provide fingerprints for the diagnosis, monitoring, and treatment of diseases.[1−8] Among established biomarker sensing techniques, including fluorescence, enzyme-linked immunosorbent assays (ELISAs), and surface plasmon resonance, electrochemical approaches offer several desirable advantages, such as miniaturization, low cost, and fast response times.[9−12] Electrochemical sensors are also capable of achieving very high sensitivity, with attomolar limits of detection having been attained by nanostructuring electrode surfaces using metal/metal oxide nanoparticles, carbon nanotubes, graphene, or conducting polymers.[13−16] Together, these characteristics have led to the widespread adoption of electrochemical sensing platforms in point-of-care (POC) and self-monitoring applications, such as blood glucose monitoring for diabetes.[10]

Despite their potential, the performance of electrochemical sensing platforms for sensing small molecule biomarkers (<1 kDa) is comparatively worse than for macromolecular biomarkers.[11,17,18] In direct electrochemical sensing platforms, where the analyte is directly oxidized or reduced at the electrode surface, the high redox stability of small molecules requires large overpotentials to activate redox reactions involved in sensing.[10,11] Small molecules are also less structurally complex than macromolecules. Together, these

Received: May 11, 2022
Revised: August 10, 2022
Accepted: August 10, 2022
Published: October 17, 2022

https://doi.org/10.1021/jacsau.2c00291
JACS Au 2022, 2, 2481−2490

factors reduce sensor selectivity. Electrochemical biosensors, which use a biological recognition element coupled to an electrochemical transduction principle, solve this issue of selectivity by relying on the ligand specificity of biomolecules.[10,14,19] Catalytic biosensors make use of an enzyme or other redox mediators, such as metal complexes,[11] to perform a secondary electron transfer reaction with the analyte. However, these biosensors are difficult to generalize (with some exceptions)[20] and can produce undesirable side products that can interfere with sensing.[21−23]

In contrast, electrochemical biosensors that use a bioreceptor, such as an antibody or aptamer, to bind the target of interest to the electrode surface do not require target-specific chemical reactions to function.[19] Once captured, the target can be detected using either an external redox probe that reports on surface accessibility or an internal probe that reports on bioreceptor morphology.[24] While antibody-based sensors are effective for sensing large macromolecular targets, the small structural changes induced by small molecule ligand binding are generally not sufficient to allow detection at the required low concentrations. In addition, aptamers are difficult to select for a specific electrochemical response[25] and can be poorly stable in biological media due to varying susceptibilities to nucleases.[26]

We overcame the challenges related to current electrochemical small molecule sensing platforms by developing a novel approach that can allow selective and sensitive electrochemical detection of small molecules. We demonstrate a new transduction amplification principle that exploits conformational changes in a dynamic bioreceptor protein to enhance the electrochemical response induced by the binding of a small molecule. As proof of this concept, we have engineered solute binding protein (SBP)-based bioreceptors specific to the detection of the amino acids leucine and glycine, two important metabolic biomarkers,[7,8] and bound them on commercially available screen-printed electrodes. While an SBP, maltose-binding protein, was previously used in the design of an electrochemical sensor, site-specific Ru(II)-labeling of the protein was required, and the resulting sensor presented a limited sensing range for maltose concentrations that spanned only 1 to 2 orders of magnitude.[27] Our sensing platforms for leucine and glycine are capable of specifically detecting their target ligands over at least 5 orders of magnitude of concentration and at concentrations as low as 1 nM and 100 nM, respectively. Given the high specificity of SBPs and their ease of modification toward a target small molecule, our sensor platform overcomes the issue of poor specificity and the need for complex electrode modifications inherent to previously introduced electrochemical small analyte detection platforms.[11]

RESULTS

Design of a Binding-Protein-Based Electrochemical Biosensor

The challenge of designing an electrochemical small molecule biosensor that is modular and generalizable is substantial. We have overcome this challenge by exploiting the large conformational changes that are intrinsic to many small molecule binding proteins, such as the SBP superfamily. Unlike ligand binding to currently widely static bioreceptors, such as antibodies, the small change in relative mass induced by analyte binding to a dynamic bioreceptor can be transduced into a large shape change. This shape change amplifies the change in available electrochemical redox sites on an electrode surface, which is quantified with an external redox probe, and provides a tunable and highly sensitive electrochemical platform for sensing small molecules (Figure 1). Moreover,

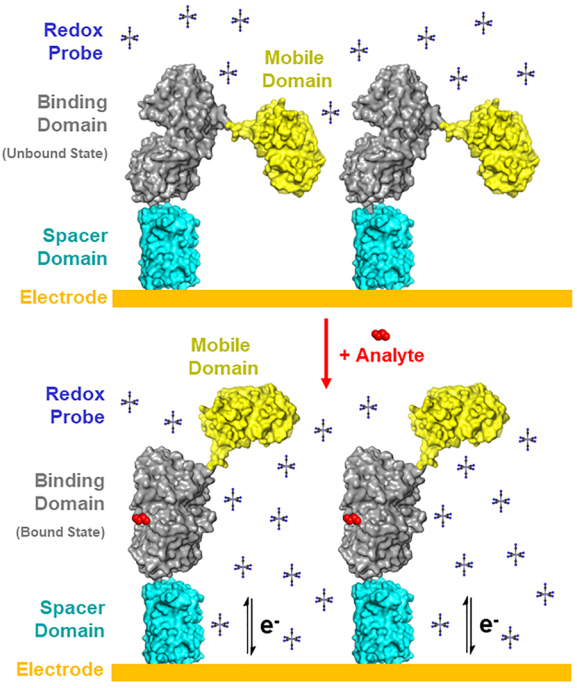

Figure 1. Schematic of the electrochemical sensing mechanism using a dynamic binding-protein-based bioreceptor. This bioreceptor consists of three domains: a binding domain (gray) that undergoes a conformational change upon binding of its ligand (red), a mobile domain (yellow) that amplifies the change in protein geometry, and a spacer domain (cyan) that prevents steric hindrance by the electrode surface (gold). Sensing occurs using a redox probe (i.e., ferricyanide, blue) via a conformational change in the binding domain upon analyte binding, which alters the morphology of the sensor and its capacity to occlude the electrode surface and, thus, leads to a change in observed redox probe signal.

the shape change and interaction of the binding protein with the electrode surface can hypothetically be increased or modified by fusing additional rigid domains to a dynamic binding protein core. For example, a protein domain could be fused to the free terminus, which we term the mobile domain, thus allowing it to be moved through space upon analyte binding to amplify the effect of the conformational change. Alternatively, a protein domain could be inserted between the binding core and the point of immobilization to the electrode surface, which we term a spacer domain, to prevent the solid surface from sterically hindering either analyte binding or the bioreceptor conformational change.

We constructed this bioreceptor by reengineering two FRET sensors for use in our electrochemical platform: one based on *Escherichia coli* LivK, a leucine-binding SBP,[28,29] and the second based on Atu2422 AYW, an engineered glycine-binding SBP previously used to engineer the GlyFS optical biosensor.[30] These SBPs both undergo a large conformational change upon ligand binding, which provides the impetus needed for transduction of the binding event. While fluorescent properties are not necessary for electrochemical sensing, the fluorescent proteins in GlyFS serve as spacer and mobile domains because

https://doi.org/10.1021/jacsau.2c00291
JACS Au 2022, 2, 2481−2490

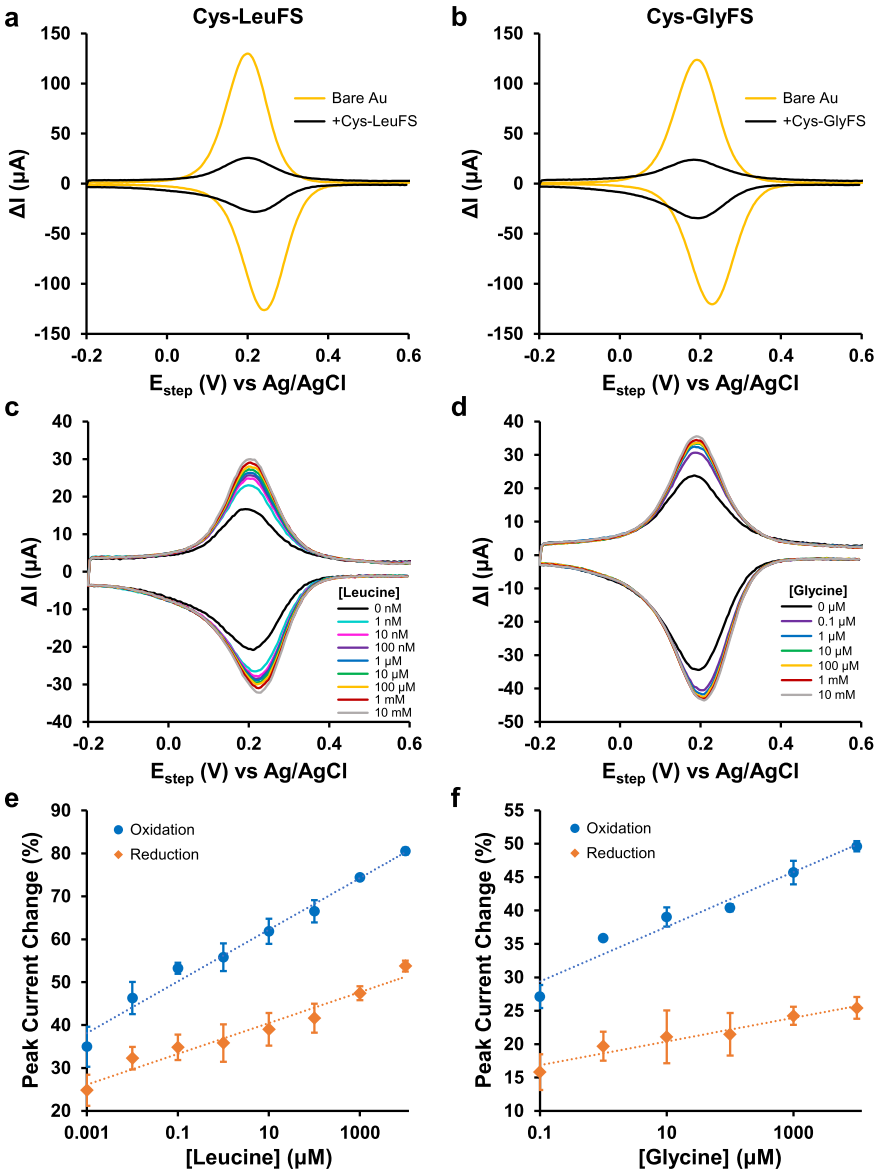

Figure 2. Electrochemical functionalization and sensing responses of Cys-LeuFS and Cys-GlyFS proteins on Au electrodes. Differential pulse voltammograms of Au screen-printed electrodes (Au SPE) functionalized with Cys-LeuFS (a) and Cys-GlyFS (b) show a decrease in ΔI compared with bare electrodes. This signal decrease is consistent with a decrease in electron transfer of the ferricyanide (5 mM) redox couple due to increased electrode surface occlusion by immobilized protein. Both the Cys-LeuFS (c) and Cys-GlyFS (d) sensors show an increase in ΔI of 5 mM ferricyanide when exposed to different concentrations of glycine and leucine, respectively. The increase in redox currents is attributed to the conformational change that arises because of binding of the amino acids to the core of the protein causing the two fluorescent probes to move apart. Panels (e) and (f) show the calibration plots of both the oxidation and reduction peak currents obtained from (c) and (d), respectively. All experiments were performed in duplicate, and the average and standard deviation are reported for each data point.

they are moderately sized, rigid, inert, and globular proteins. Their use also allows the benchmarking of our constructs' analyte binding properties using well-established fluorescence-based characterization methods. Therefore, enhanced cyan fluorescent protein (ECFP) was used as a spacer domain and fused directly to the N-terminus of the SBPs, and Venus was used as a mobile domain and fused to the C-terminus using the previously optimized $(EAAAK)_3$ rigid linker from GlyFS.[30] A hexa-histidine tag (His-tag) was fused to the C-terminus of Venus for protein purification using a flexible GGS linker. A tricysteine tag (Cys-tag) was also fused to the N-terminus of the ECFP domain using a flexible $(GGS)_2$ linker, which allowed for covalent attachment of the sensor to the surface of a gold electrode through a sulfhydryl-gold reaction (Figures S1 and S2). This functionalization strategy allows for the direct and oriented attachment of the sensor to the electrode surface,[31] which is an important consideration due to the short range of probe−electrode interactions and the anisotropic nature of bioreceptor−electrode interactions.

The electrodes were functionalized by first heterologously expressing the two constructs, termed Cys-LeuFS and Cys-GlyFS for the leucine-binding and glycine-binding sensors, respectively, in *E. coli* and purifying them through a combination of Ni^{2+}-NTA affinity chromatography and size-exclusion chromatography (Figures S3 and S4). Gold screen-printed electrodes (Au SPEs) were used because of their low cost and potential for miniaturization.[32,33] Following electrode functionalization, we confirmed by using scanning electron

https://doi.org/10.1021/jacsau.2c00291
JACS Au 2022, 2, 2481−2490

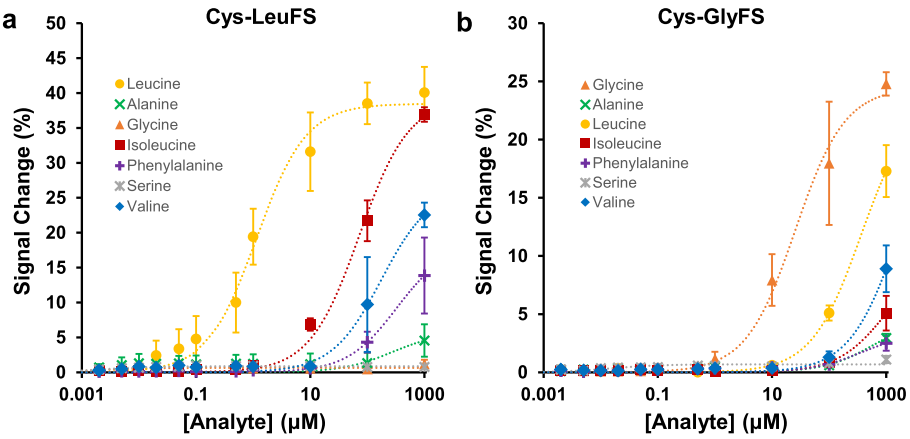

Figure 3. Fluorescence sensing responses of Cys-LeuFS and Cys-GlyFS. Fluorescence dose−response curves of Cys-LeuFS (a) and Cys-GlyFS (b) to a panel of amino acids including both on- and off-target ligands. Nonlinear regressions (dotted lines) were used to fit 2-term saturation binding models. Signal change was determined using the ECFP/Venus emission peak ratio (475 nm/530 nm) relative to signal in absence of any amino acids in solution. All experiments were performed in triplicate, and the average and standard deviation were reported for each data point.

microscopy that no large aggregates of insoluble material or fouling layer had deposited on the electrodes (Figure S5). Next, we measured the extent of electrode functionalization with Cys-LeuFS and Cys-GlyFS using differential pulse voltammetry (DPV)—a highly sensitive electroanalytical technique.[34,35] A DPV scan with a bare Au SPE immersed in a ferricyanide solution produced a pair of peaks corresponding to the $Fe^{2+/3+}$ redox couple. In contrast, a reduction in the redox peak currents by 70−80% was observed after attachment of either construct (Figure 2), which is indicative of a reduction of redox probe diffusion by the bound protein. This decrease in current was stable over several successive scans, which is consistent with the expected covalent binding of the bioreceptor to the electrode. In addition, the peak-to-peak separation of roughly 40 mV of the bare AuSPEs was reduced, which is known to occur when conductance through surface-bound proteins accelerates electron transfer kinetics to the probe.[36,37]

Electrochemical Sensing Using a Protein Conformational Change

The sensitivity of these biosensors was assessed *in vitro* through differential pulse voltammograms (DPV) using ferricyanide solutions spiked with leucine or glycine at concentrations reflecting the solution-state binding affinities of each respective sensor [LivK K_D (Leu) = 8 μM; Atu2422 AYW K_D (Gly) = 20 μM].[29,30] Exposure of both Cys-LeuFS and Cys-GlyFS to their respective target analytes resulted in an analyte-concentration-dependent increase in measured current (Figure 2c,d). Conversely, in a control using unfunctionalized electrodes exposed to analyte concentrations of 1 μM to 10 mM, we observed either no change in signal at analyte concentrations of 100 μM or lower or a decrease in signal at higher analyte concentrations (Figure S6). This may indicate that the analytes are capable of adsorption to the electrode surface at high concentration. However, this results in a loss of signal, which indicates that the gain in signal observed when using functionalized electrodes is a result of the intended sensing mechanism rather than nonspecific adsorption. The observed change in current is also unlikely to have been caused by changes in the redox states of leucine and glycine, which are electrochemically inert over the potential ranges used. Thus, the observations of analyte-concentration-dependent changes in current when using these sensors are most likely due to the protein conformational changes upon ligand binding increasing electrode surface accessibility. A major advantage of this signaling mode is the gain-of-signal detection mode induced in comparison with the loss-of-signal modes that are used by many immuno- and DNA-based electrochemical sensors.[9,19]

For both sensors, the oxidation peak current produces a bigger percent signal change compared with the reduction peak current. The oxidation peak current could, therefore, be used as the analytical signal despite the use of ferricyanide as redox probe, which first undergoes a reduction reaction during potential cycling. The difference between responses could be due to the retention of probe molecules at the electrode surface by the protein layer. The diffusion of ferrocyanide away from the surface and into the bulk solution leads to a lower basal oxidation peak current relative to the reduction peak current, as seen in Figure 2c,d. Retention of the probe as a result of bioreceptor conformational changes would, therefore, allow for a recovery of the oxidation peak when the polarity is reversed and result in a higher observed sensitivity relative to its initial lower baseline.

The sensors' responses to their respective targets were then measured through generation of calibration curves for each sensor. Both sensors exhibited similar relatively log−linear increases in current for both DPV redox peaks over the range of analyte concentrations tested (Figure 2e,f). The Cys-LeuFS detection range for leucine concentration was shown to range at least 7 orders of magnitude, from as low as 1 nM (the lowest concentration tested on the basis of the estimated Cys-LeuFS K_D) to as high as 10 mM (close to the leucine solubility limit), with estimated lower limits of detection of 2 pM and 4 pM for the DPV oxidation and reduction peaks, respectively, and with a maximal signal change of at least 50% and 80% for the DPV reduction and oxidation peaks, respectively. Similarly, Cys-GlyFS was capable of quantitatively sensing glycine concentrations over at least 5 orders of magnitude, from as low as 100 nM (the lowest concentration tested on the basis of the estimated Cys-GlyFS K_D) to as high as 10 mM, with estimated lower limits of detection of 2 pM and 200 pM for the DPV oxidation and reduction peaks, respectively, and with a maximal signal change of at least 25% and 50% for the DPV reduction and oxidation peaks, respectively. In contrast to these electrochemical sensing results, evaluation of the

https://doi.org/10.1021/jacsau.2c00291
JACS Au 2022, 2, 2481−2490

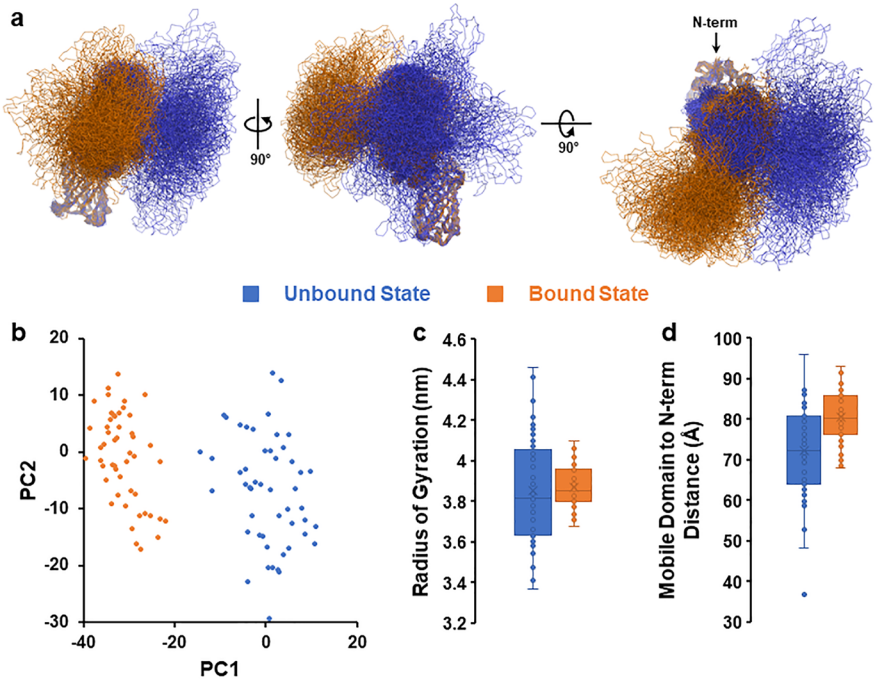

Figure 4. Cys-LeuFS modeling results. (a) Conformational ensembles of 50 members each for both the unbound (blue) and ligand-bound (orange) states were generated using molecular dynamics simulations with the MARTINI coarse-grain force field[40] to equilibrate fusion protein models over 100 ns simulations. Each ensemble member represents the final frame of an independent simulation replicate. The position of the construct N-terminus is indicated in the third orientation to highlight the surface attachment point. (b) A principal component analysis of the combined conformational ensemble demonstrates separation of both conformational states along PC1, which indicates that both states adopt distinct and separable conformations. (c) An analysis of radius of gyration for each ensemble member, shown here as a box plot, shows a broader distribution of radii of gyration for the unbound state in comparison with the ligand-bound state. Because radius of gyration is a function of molecular geometry, this is indicative of increased conformational plasticity in the unbound state. (d) Box plots of the distance between the mobile domain center of mass to the construct N-terminus (an approximation of distance between the mobile domain and the electrode surface following functionalization) show that the unbound state populates conformations that bring the mobile domain closer to the hypothetical surface location.

performance of these sensors as optical FRET sensors (Figure 3, Figure S7) showed the expected sigmoidal dose response curves with dynamic ranges of roughly 25−40% and concentration ranges of approximately 3 orders of magnitude, similar to what has previously been observed for SBP-based FRET biosensors.[29,30] Both our leucine and glycine sensors, therefore, display enhanced signal changes and concentration detection ranges when used in electrochemical, as opposed to optical, platforms.

The different response characteristics of Cys-LeuFS and Cys-GlyFS as electrochemical and optical sensors can be explained by the respective theoretical molecular mechanisms of these two modes. FRET biosensor signaling is dominated by bioreceptor−ligand interactions, where the measured signal is the aggregate of signals produced by each bioreceptor upon binding of a ligand molecule. As these binding events and the resulting FRET signal are substantially independent across bioreceptor molecules, the sensor's optical response therefore follows a simple two-state noncooperative saturation binding model.[29,30] Signaling from the electrochemical sensor, however, depends instead on accessibility of the electrode surface to the external redox probe. This morphological element is a considerably more complex combination of factors than independent bioreceptor−probe binding, as bioreceptor molecules interact both together and with redox probe molecules during signal transduction. As a result, it is possible that transient binding events at low analyte concentrations that are below the K_D of the bioreceptor by several orders of magnitude and would not be detected in the optical sensing mode could quantifiably affect interaction between bioreceptor molecules. Such a mechanism could therefore explain the broadened effective concentration range observed for the electrochemical sensing mode.

Molecular Basis of the Sensing Mechanism

We probed the nature of these interactions in order to better understand the molecular mechanism underpinning these sensors' response by examining the roles of the static and mobile domain of the probes in this mechanism. Truncation of either domain results in considerably worse sensor performance (Figure S8). Specifically, after the spacer domain was truncated, the analytical signal of the sensor decreased by over 85% relative to the signal generated by the complete construct. This loss of sensor response suggests that this domain is required to mitigate surface proximity effects, such as steric hindrance, that can impede ligand-binding-driven conformational changes in the sensor. Similarly, truncation of the mobile domain decreased the sensor response by nearly 75% relative to the complete construct and led to a loss-of-signal detection mode. This observation is consistent with the comparatively smaller closing motion that the SBP binding domain undergoes upon ligand binding in comparison with the global opening motion that occurs when the mobile domain is present and is responsible for sensor signaling.

We further examined the protein conformational change that occurs upon ligand binding to the sensor by generating conformational ensembles of Cys-LeuFS in both the leucine-bound and unbound states using an established coarse-grained

https://doi.org/10.1021/jacsau.2c00291
JACS Au 2022, 2, 2481−2490

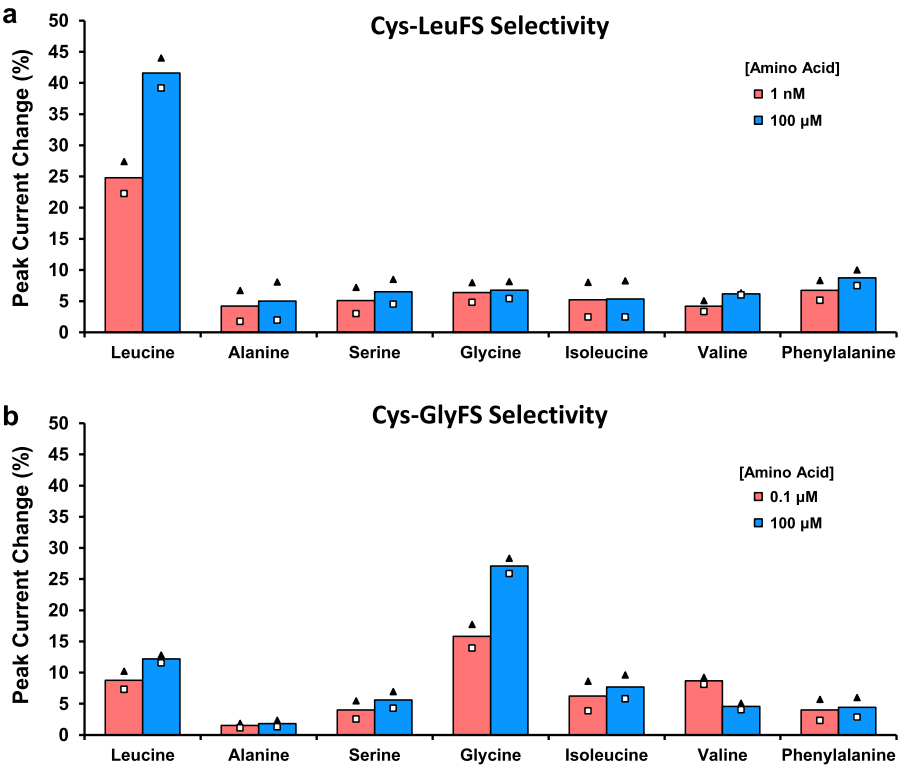

Figure 5. Bar plots depicting selectivity of Cys-LeuFS and Cys-GlyFS against selected amino acids. Selectivity bar plots showing the differential pulse voltammetry response of Cys-LeuFS (a) and Cys-GlyFS (b) to a panel of 7 free amino acids including both on- and off-target analytes. The signal change was determined at the reduction peak, relative to the signal in the absence of any amino acids in solution. All experiments were performed in duplicate, with the bar showing the average of both replicates, and results for the two replicates shown separately as black triangles or white squares, respectively.

modeling algorithm (Figure 4a, Figures S9 and S10).[38] The resulting ensembles demonstrate that both states adopt distinct and separable conformational spaces (Figure 4b). In addition, a solvent exclusion volume analysis[39] demonstrates that the leucine-bound and unbound states differ in total volume by <1% (Figure S11). These results corroborate that a shape effect rather than a volume or size effect is likely responsible for the observed signal changes upon analyte binding. Further examination of the geometry of these ensemble members shows that while both states exhibit fluctuations of similar magnitudes during equilibration (Figure S12), the protein's unbound state can adopt a wider range of conformations, as evidenced by the broader distributions for both radius of gyration (Figure 4c) and the first four principal component projections (Figure S13). This conformational plasticity could allow protein molecules in the unbound state to adopt conformations that more readily occlude the electrode surface. Indeed, we observed through examination of the distance between the mobile domain center of mass and the construct's N-terminus (the location of the surface attachment point) that both the average and minimum distance is considerably reduced for proteins in the unbound state compared with the bound state (Figure 4d). This further suggests that in their unbound state, our bioreceptors more strongly inhibit redox probe diffusion to the electrode surface than in their more compact bound state, which helps to explain the molecular basis for our sensors' function.

Given the dynamic nature of this shape-change sensing mechanism, we next verified the reversibility of analyte binding by Cys-GlyFS over repeated measurements by cycling between ferricyanide solutions containing either no glycine or one of two concentrations of glycine (Figure S14). Although signal changes and, therefore, analyte binding were substantially reversible, a progressive baseline shift was observed over multiple measurements, reaching a plateau after the third return to the glycine-free solution. This baseline shift does not occur in the absence of a functionalized protein layer on the electrode and is, therefore, most likely related to a change in the morphology of the bioreceptor layer during initial exposure to the analyte. Despite this baseline shift, which may be resolved by a priming step given the rapid plateau attained, the sensor nevertheless remained active and responsive to changes in glycine concentration over all measurements, and the elevated baseline remained below the level of sensor response to even a low glycine concentration. This is attributed to the reversible nature of SBP ligand binding and suggests that the sensor could be used for continuous monitoring applications following additional optimization and/or calibration steps.

Selective Small Molecule Electrochemical Sensor

We have demonstrated the excellent and tunable selectivity of our sensor platform by using amino acids as target analytes because they present a high level of similarity and are known to be very difficult to discriminate between by established approaches.[11] Thus, the selectivity of our glycine- and leucine-sensing platforms was assessed against a panel of other common amino acids, including polar, nonpolar, small, and bulky amino acids. An initial validation using optical (FRET) sensing showed that Cys-LeuFS was selective for leucine, with some weaker affinity for isoleucine and valine, while Cys-GlyFS was selective for glycine, with some weak affinity for leucine and valine (Figure 3). We then tested our

https://doi.org/10.1021/jacsau.2c00291
JACS Au 2022, 2, 2481−2490

electrochemical sensing platform's ability to selectively sense these amino acids using the same panel of amino acids at both a low concentration (1 nM for Cys-LeuFS and 100 nM for Cys-GlyFS) and a high concentration (100 μM for both sensors) (Figure 5, Figures S15 and S16). The Cys-LeuFS-functionalized sensors demonstrated high selectivity for leucine, with the off-target signal observed at high concentrations of isoleucine or valine in optical sensing being largely absent in electrochemical sensing. This alteration to bioreceptor selectivity is likely the result of its surface immobilization, which could hinder adoption of rare conformations that promote off-target binding.

The Cys-GlyFS-functionalized sensors displayed the highest response for glycine, with some affinity for leucine and valine. While the trend in terms of selectivity is consistent with the FRET data, it is notable that the sensitivity appears to be greater when the proteins are used as part of our electrochemical sensing platform; a > 20% current change for Cys-LeuFS in the presence of 1 nM leucine, with selective detection over 7 orders of magnitude (1 nM - 10 mM), is remarkable. Most importantly, the ligand-binding domain of these sensors is the only domain that differs between both platforms. We can thus conclude that the different selectivity observed for these sensors (Cys-LeuFS vs Cys-GlyFS) indicates that the platform's selectivity is dictated by the ligand-binding domain and that swapping this domain for another with a different ligand selectivity, in a modular fashion, is sufficient to alter the selectivity of the biosensor.

DISCUSSION

In this work, we developed a novel protein-based electrochemical biosensor platform, exemplified by two amino acid biosensors, Cys-LeuFS and Cys-GlyFS, which harness a protein conformational change as a transduction mechanism to detect a small molecule. This was accomplished by reengineering two SBP-based optical biosensors, resulting in a marked increase in the sensors' effective concentration range and sensitivity upon translation to an electrochemical detection platform. These sensors' properties can solve several major issues in electrochemical sensing of small molecules, where large overpotentials and low selectivity are commonplace.[11] In addition to these direct advantages in sensing, the modular nature of these novel sensors, where the core bioreceptor dictates selectivity, makes them appealing for future engineering and diversification efforts. Notably, this work lays out the foundation for readily creating a family of other SBP-based electrochemical biosensors by harnessing the breadth of ligand specificity found in this protein family.[41−44] This process is facilitated by the less strict geometries required in electrochemical sensing relative to the optimization of FRET efficiency changes in optical sensing, the latter of which often requires extensive linker optimization.[30] The ability to directly translate optical FRET sensors to electrochemical sensors also benefits efforts to target new ligands not yet represented by existing SBPs, as optical sensors are particularly amenable to protein engineering efforts due to the availability of high-throughput optical screening methods.[45,46] Therefore, our available toolbox of electrochemical biosensors could readily be expanded by engineering optical SBP-based sensors with altered ligand selectivity or affinity and then translating these into broadly applicable and highly sensitive electrochemical platforms.

Beyond modifications to our biosensors' selectivity, considerable room for future optimization of these sensors' response remains. While the demonstrated effective concentration range is already well suited to applications such as environmental sensing, where variations in target concentration of several orders of magnitude are relatively common, our sensors' resolution is still relatively low. Optimization of the size, shape, and net charge of their mobile and static domains, which consequently changes the electrochemical morphology of the sensor, would further enhance the signal change observed upon analyte binding to enhance both sensitivity and resolution. In this work, we also used only the ferri-/ferrocyanide inner sphere redox probe system to benchmark the sensing platform. Additional mechanistic or optimization studies could use other redox probes such as ferrocene or RuHex, which are outer sphere probes, to further understand probe diffusion properties and optimize the platform's sensitivity. In addition, the inclusion of filtration or antifouling layers in the sensor construction could allow for compatibility with complex biological media. Despite these avenues for future improvement, the ability of these protein-based bioreceptors to selectively capture and detect small molecule targets is already a significant advancement compared with current methods that rely on using electrocatalysts or redox mediators. Both of these existing approaches can lack selectivity, especially toward structurally simple molecules such as glycine.[11] Cys-LeuFS and Cys-GlyFS are instead capable of discriminating their respective native ligands leucine and glycine from other chemically similar chain amino acids, which highlights the exquisite specificity that can be attained using binding proteins as bioreceptors.

Overall, we have shown how highly sensitive and specific electrochemical biosensors can be developed by integrating dynamic binding-protein-based bioreceptors with highly sensitive electro-analytical techniques. This novel platform opens avenues for the detection of small molecules, such as leucine and glycine, which are two medically relevant amino acids that are involved in key biological functions yet can be difficult to sense using small footprint sensing platforms. Future optimization of our biosensors' protein elements and the ready miniaturization of the platform enabled using SPEs bears potential for a large range of applications, including their use as miniaturized sensors for portable and point-of-care medical, diagnostic, and environmental monitoring.

MATERIALS AND METHODS

Gene Constructs and Cloning

Cys-LeuFS and Cys-GlyFS constructs were designed by sequential fusion of three protein domains. The N-terminal domain consists of ECFP with an N-terminal Cys-tag and a 9 amino acid truncation at its C-terminus to remove the flexible ECFP C-terminal tail. This ECFP construct was fused to a leucine-binding (*E. coli* LivK) or glycine-binding (Atu2422 AYW) solute binding protein from which the signal peptide was truncated, which was in turn fused to a C-terminal Venus domain using the rigid linker $(EAAAK)_3$. Codon-optimized genes for Cys-LeuFS and Cys-GlyFS cloned into the pET-29b(+) and pET-28a(+) vectors, respectively, were obtained from Twist Biosciences and transformed via electroporation into *E. coli* BL21(DE3).

Protein Expression and Purification

Proteins were expressed using an autoinduction medium (yeast extract, 5 g/L; tryptone, 20 g/L; NaCl, 5 g/L; KH_2PO_4, 3 g/L; Na_2HPO_4, 6 g/L with 10 mL/L 60% (v/v) glycerol, 5 mL/L 10% (w/v) glucose, and 25 mL/L 8% (w/v) lactose) supplemented with 50

https://doi.org/10.1021/jacsau.2c00291
JACS Au 2022, 2, 2481−2490

mg of kanamycin or 100 mg of ampicillin for Cys-LeuFS or Cys-GlyFS expression, respectively. Cultures were grown at 18 °C with shaking for 72−96 h with periodic monitoring of ECFP and Venus fluorescence to gauge protein expression. Following growth, cells were harvested by centrifugation and stored at −20 °C. For purification, the frozen pellet was suspended in buffer A (50 mM sodium phosphate, 300 mM NaCl, 20 mM imidazole, pH 7.4), lysed by sonication, recentrifuged at high speed (22 400*g* for 60 min at 4 °C) and the cleared supernatant was collected. This was loaded onto a 5 mL Ni-NTA/His-trap column pre-equilibrated in buffer A, washed with 10 column volumes of buffer A, followed by 5 column volumes of 10% buffer B, and eluted with 100% buffer B (50 mM sodium phosphate, 300 mM NaCl, 250 mM imidazole, pH 7.4), and the eluted sensor protein was dialyzed against 3 exchanges of 4 L of buffer C (20 mM sodium phosphate, 200 mM NaCl, pH 7.4) at 4 °C. The dialyzed protein was further purified using a GE Healthcare HiLoad 26/600 Superdex 200 pg SEC column using buffer C. Protein purity was confirmed by SDS-PAGE, and protein concentrations were measured spectrophotometrically using predicted molar absorption coefficients.

Fluorescence Assays

Fluorescence titrations were performed using a Cary Eclipse fluorimeter (Varian) using a 1 cm quartz narrow volume fluorescence cuvette (Hellma Analytics). Protein samples containing 2 uM Cys-LeuFS or Cys-GlyFS and 0.001 μM to 1000 μM free amino acids (leucine, glycine, alanine, valine, isoleucine, serine, and phenylalanine) in buffer C (20 mM sodium phosphate, 200 mM NaCl, pH 7.4) underwent excitation at 433 nm, and emission scans from 450 to 560 nm were obtained in triplicate with a step size of 1 nm. ECFP/Venus fluorescence ratios were determined using fluorescence intensities at 475 nm (ECFP emission peak) and 530 nm (Venus emission peak). K_D values were determined by fitting curves through nonlinear regression using a saturation binding model:

$$y = \frac{y_{min} + [L] \times (y_{max} - y_{min})}{K_D + [L]}$$

where $[L]$ represents concentration of ligand in solution, and y represents fluorescent signal.

Electrochemical Methods

All electrochemical experiments were performed using a VMP3 potentiostat (BioLogic) interfaced to a PC with EC-Lab software. Au SPEs (Au AT, Dropsens) were first cleaned in 0.1 M H_2SO_4 (Sigma-Aldrich) by cycling between 0 and 1.4 V for 10 times at a scan rate of 1 V/s. Following this, they were dipped in a solution of 5 mM $K_3Fe(CN)_6$ (Sigma-Aldrich) in phosphate-buffered saline (20 mM sodium phosphate, 200 mM NaCl, pH 7.4) and scanned between the potential range from −0.2 to 0.6 V versus Ag/AgCl using differential pulse voltammetry (DPV) with an amplitude of 0.05 V, modulation time of 0.05 s, and interval time of 0.1 s. Once stable redox peaks characteristic of the $Fe^{2+/3+}$ couple were seen, the SPEs were removed, washed with DI, and then dried before drop casting 100 μL of Cys-LeuFS/Cys-GlyFS for 3 h. This functionalized surface was dipped back into 5 mM $K_3Fe(CN)_6$/phosphate-buffered saline to record following DPVs. The electrodes were then exposed to different concentrations of amino acids (leucine, glycine, alanine, valine, isoleucine, serine, or phenylalanine from Sigma-Aldrich) with DI washing steps before and after every exposure. Au/Pt thin-film electrodes (Micrux) were cleaned in 0.05 M H_2SO_4 (Sigma-Aldrich) by cycling between −1 and 1.3 V for 50 times at a scan rate of 100 mV/s and utilized as above, albeit with a potential range from −0.5 to 0.3 V versus Pt and a functionalization time of 2 h. Lower limits of detection were estimated from these data as the target concentration, where the extrapolated percent signal change corresponds to 3.3 standard deviations of the regression.[47]

Scanning Electron Microscopy

The morphology of the Au screen-printed electrodes was investigated using a field-emission scanning electron microscope Zeiss Ultra Plus (operating at 3 kV) without coating.

Construct Modeling

Starting structures were generated in PyMOL[48] by fusing unbound and ligand-bound LivK (PDB ID: 1USG and 1USK, respectively)[49] directly to ECFP (PDB ID: 5OX8)[50] and to Venus (PDB ID: 1MYW)[51] using a fully extended $(EAAAK)_3$ linker. Coarse-grained simulations were prepared by solvating starting structures in a dodecahedral solvent box with a minimum distance of 10 Å from any protein atom to the box wall, followed by coarse-graining using the Martinize script. Coarse-grained simulations were run in GROMACS[52] using the MARTINI force field.[40] Structures were first minimized using steepest-descent energy minimization, followed by a 100 ps equilibration in the NVT ensemble and a 100 ps equilibration in the NPT ensemble. Structure equilibration including linker collapse was carried out over 50 replicate trajectories of 100 ns for each state, with a 2.5 fs time step and an elastic network model used to maintain domain geometry with restraints on linker beads removed to allow free equilibration of the linker. Temperature coupling used a V-rescale thermostat and pressure coupling used a Parinello−Rahman barostat. Following equilibration, coarse-grained structures were converted back to fine-grained models using the Backward tool.[53] Geometry analysis was carried out in VMD,[54] solvent exclusion volume was calculated using ProteinVolume 1.3,[39] and PCA analysis was carried out using PRODY.[55]

■ ASSOCIATED CONTENT

Supporting Information

The Supporting Information is available free of charge at https://pubs.acs.org/doi/10.1021/jacsau.2c00291.

Construct sequences, size-exclusion chromatograms, SDS-PAGE gels, scanning electrode micrographs, additional controls, fluorescence spectra, characterization of truncated variants, analysis of molecular dynamics simulations, reversibility experiments, differential pulse voltammograms of selectivity tests (DOCX)

■ AUTHOR INFORMATION

Corresponding Authors

Colin J. Jackson − *Research School of Chemistry, Australian Research Council Centre of Excellence for Innovations in Peptide and Protein Science, Research School of Chemistry, and Australian Research Council Centre of Excellence in Synthetic Biology, Research School of Chemistry, The Australian National University, Canberra, ACT 2601, Australia;* orcid.org/0000-0001-6150-3822; Email: colin.jackson@anu.edu.au

Antonio Tricoli − *Nanotechnology Research Laboratory, Research School of Chemistry, College of Science, The Australian National University, Canberra, ACT 2601, Australia; Nanotechnology Research Laboratory, Faculty of Engineering, University of Sydney, Sydney, NSW 2006, Australia;* Email: antonio.tricoli@sydney.edu.au

Authors

Krishnan Murugappan − *Nanotechnology Research Laboratory, Research School of Chemistry, College of Science, The Australian National University, Canberra, ACT 2601, Australia; CSIRO, Mineral Resources, Clayton South, VIC 3169, Australia;* orcid.org/0000-0002-6845-4653

https://doi.org/10.1021/jacsau.2c00291
JACS Au 2022, 2, 2481−2490

Uthayasuriya Sundaramoorthy − *Research School of Chemistry, The Australian National University, Canberra, ACT 2601, Australia*

Adam M. Damry − *Research School of Chemistry, The Australian National University, Canberra, ACT 2601, Australia; Department of Chemistry and Biomolecular Sciences, University of Ottawa, Ottawa, ON K1N 6N5, Canada;* orcid.org/0000-0003-3596-3133

David R. Nisbet − *Laboratory of Advanced Biomaterials, Research School of Chemistry and the John Curtin School of Medical Research, The Australian National University, Canberra, ACT 2601, Australia; The Graeme Clark Institute and Department of Biomedical Engineering, Faculty of Engineering and Information Technology, The University of Melbourne, Melbourne, VIC 3010, Australia;* orcid.org/0000-0002-1343-0769

Complete contact information is available at: https://pubs.acs.org/10.1021/jacsau.2c00291

Author Contributions

¶K.M., U.S., and A.M.D. contributed equally to this work. A.M.D., A.T., C.J.J., D.R.N., and K.M. conceptualized the electrochemical platform. A.M.D., C.J.J., and U.S. designed and optimized the platform's protein elements. A.T. and K.M. designed and optimized the platform's electrochemical elements. U.S. expressed the protein and performed and analyzed fluorescence characterization experiments. K.M. performed scanning electron microscopy experiments, performed electrochemical sensing experiments, and analyzed electrochemical sensing data. A.M.D. generated and analyzed bioreceptor computational models. A.M.D., A.T., C.J.J., and D.R.N. obtained funding for the project. A.M.D., A.T., C.J.J., and K.M. wrote the manuscript. All authors reviewed the manuscript.

Notes

The authors declare no competing financial interest.

The main data supporting the findings of this study are available within the paper and its Supporting Information. Any other relevant data are available from the corresponding authors upon reasonable request. Source data are provided with this paper.

ACKNOWLEDGMENTS

This research was funded by and has been delivered in partnership with Our Health in Our Hands (OHIOH), a strategic initiative of the Australian National University, which aims to transform healthcare by developing new personalized health technologies and solutions in collaboration with patients, clinicians, and health care providers. A.T. gratefully acknowledges the support of the Australian Research Council for a Future Fellowship (FT200100939) and a Discovery grant DP190101864 and the support from the North Atlantic Treaty Organization Science for Peace and Security Programme project AMOXES (#G5634). D.R.N was supported by a NHMRC Research Leadership Fellowship (GNT1135657). A.M.D. acknowledges funding from the Human Frontier Science Program (LT-000366/2020-C). Funding by the Australian Research Council Centre of Excellence for Innovations in Peptide and Protein Science and the Centre of Excellence in Synthetic Biology is gratefully acknowledged. This project was undertaken with the assistance of resources and services from the National Computational Infrastructure (NCI), which is supported by the Australian Government.

REFERENCES

(1) Pandi-Perumal, S. R.; Trakht, I.; Srinivasan, V.; Spence, D. W.; Maestroni, G. J. M.; Zisapel, N.; Cardinali, D. P. Physiological effects of melatonin: Role of melatonin receptors and signal transduction pathways. *Progress in Neurobiology* **2008**, *85* (3), 335−353.

(2) Emamzadeh, F. N.; Surguchov, A. Parkinson's Disease: Biomarkers, Treatment, and Risk Factors. *Front Neurosci* **2018**, *12*, 612−612.

(3) Glunde, K.; Serkova, N. J. Therapeutic targets and biomarkers identified in cancer choline phospholipid metabolism. *Pharmacogenomics* **2006**, *7* (7), 1109−1123.

(4) Subash, P.; Gurumurthy, P.; Sarasabharathi, A.; Cherian, K. M. Urinary 8-OHdG: A marker of oxidative stress to DNA and total antioxidant status in essential hypertension with South Indian population. *Indian Journal of Clinical Biochemistry* **2010**, *25* (2), 127−132.

(5) Okorie, O. N.; Dellinger, P. Lactate: biomarker and potential therapeutic target. *Crit Care Clin* **2011**, *27* (2), 299−326.

(6) Lytvyn, Y.; Perkins, B. A.; Cherney, D. Z. I. Uric Acid as a Biomarker and a Therapeutic Target in Diabetes. *Canadian Journal of Diabetes* **2015**, *39* (3), 239−246.

(7) Giesbertz, P.; Daniel, H. Branched-chain amino acids as biomarkers in diabetes. *Curr. Opin. Clin. Nutr. Metab. Care* **2016**, *19* (1), 48−54.

(8) Socha, E.; Koba, M.; Kośliński, P. Amino acid profiling as a method of discovering biomarkers for diagnosis of neurodegenerative diseases. *Amino Acids* **2019**, *51* (3), 367−371.

(9) Drummond, T. G.; Hill, M. G.; Barton, J. K. Electrochemical DNA sensors. *Nat. Biotechnol.* **2003**, *21* (10), 1192−1199.

(10) Wang, J. Electrochemical biosensors: Towards point-of-care cancer diagnostics. *Biosens. Bioelectron.* **2006**, *21* (10), 1887−1892.

(11) Pérez-Ràfols, C.; Liu, Y.; Wang, Q.; Cuartero, M.; Crespo, G. A. Why Not Glycine Electrochemical Biosensors? *Sensors* **2020**, *20* (14), 4049.

(12) Karawdeniya, B. I.; Damry, A. M.; Murugappan, K.; Manjunath, S.; Bandara, Y. M. N. D. Y.; Jackson, C. J.; Tricoli, A.; Neshev, D., Surface Functionalization and Texturing of Optical Metasurfaces for Sensing Applications. *Chem. Rev.***2022**. DOI: 10.1021/acs.chemrev.1c00990

(13) Walcarius, A.; Minteer, S. D.; Wang, J.; Lin, Y.; Merkoçi, A. Nanomaterials for bio-functionalized electrodes: recent trends. *J. Mater. Chem. B* **2013**, *1* (38), 4878−4908.

(14) Cho, I.-H.; Kim, D. H.; Park, S. Electrochemical biosensors: perspective on functional nanomaterials for on-site analysis. *Biomaterials Research* **2020**, *24* (1), 6.

(15) Murugappan, K.; Castell, M. R. Bridging electrode gaps with conducting polymers around the electrical percolation threshold. *Electrochem. Commun.* **2018**, *87*, 40−43.

(16) Dastidar, M. G.; Murugappan, K.; Damry, A. M.; Nisbet, D. R.; Nolan, C. J.; Tricoli, A. When Less Gold is More: Selective Attomolar Biosensing at the Nanoscale. *Adv. Funct. Mater.* **2022**, *32* (24), 2105433.

(17) Krishnan, S. Review—Electrochemical Sensors for Large and Small Molecules in Biofluids. *J. Electrochem. Soc.* **2020**, *167* (16), 167505.

(18) Pfeiffer, F.; Mayer, G.*Selection and Biosensor Application of Aptamers for Small Molecules*. 2016, *4* (25)..

(19) Felix, F. S.; Angnes, L. Electrochemical immunosensors − A powerful tool for analytical applications. *Biosens. Bioelectron.* **2018**, *102*, 470−478.

(20) Guo, Z.; Johnston, W. A.; Stein, V.; Kalimuthu, P.; Perez-Alcala, S.; Bernhardt, P. V.; Alexandrov, K. Engineering PQQ-glucose dehydrogenase into an allosteric electrochemical Ca2+ sensor. *Chem. Commun.* **2016**, *52* (3), 485−488.

(21) Carpenter, A. C.; Paulsen, I. T.; Williams, T. C. Blueprints for Biosensors: Design, Limitations, and Applications. *Genes (Basel)* **2018**, *9* (8), 375.
(22) Soleymani, L.; Li, F. Mechanistic Challenges and Advantages of Biosensor Miniaturization into the Nanoscale. *ACS Sensors* **2017**, *2* (4), 458−467.
(23) Luka, G.; Ahmad, S.; Falcone, N.; Kraatz, H.-B.23 - Advances in enzyme-based electrochemical sensors: current trends, benefits, and constraints. In *Bioelectronics and Medical Devices*; Pal, K., Kraatz, H.-B., Khasnobish, A., Bag, S., Banerjee, I., Kuruganti, U., Eds.; Woodhead Publishing, 2019; pp 555−590.
(24) Kurnik, M.; Pang, E. Z.; Plaxco, K. W. An Electrochemical Biosensor Architecture Based on Protein Folding Supports Direct Real-Time Measurements in Whole Blood. *Angew. Chem., Int. Ed.* **2020**, *59* (42), 18442−18445.
(25) Rozenblum, G. T.; Pollitzer, I. G.; Radrizzani, M. Challenges in Electrochemical Aptasensors and Current Sensing Architectures Using Flat Gold Surfaces. *Chemosensors* **2019**, *7* (4), 57.
(26) Yoo, H.; Jo, H.; Oh, S. S. Detection and beyond: challenges and advances in aptamer-based biosensors. *Materials Advances* **2020**, *1* (8), 2663−2687.
(27) Benson, D. E.; Conrad, D. W.; de Robert, M.; Lorimier, n.; Trammell, S. A.; Hellinga, H. W. Design of Bioelectronic Interfaces by Exploiting Hinge-Bending Motions in Proteins. *Science* **2001**, *293* (5535), 1641−1644.
(28) Yoshida, T.; Nakajima, H.; Takahashi, S.; Kakizuka, A.; Imamura, H. OLIVe: A Genetically Encoded Fluorescent Biosensor for Quantitative Imaging of Branched-Chain Amino Acid Levels inside Single Living Cells. *ACS Sensors* **2019**, *4* (12), 3333−3342.
(29) Mohsin, M.; Abdin, M. Z.; Nischal, L.; Kardam, H.; Ahmad, A. Genetically encoded FRET-based nanosensor for in vivo measurement of leucine. *Biosens. Bioelectron.* **2013**, *50*, 72−77.
(30) Zhang, W. H.; Herde, M. K.; Mitchell, J. A.; Whitfield, J. H.; Wulff, A. B.; Vongsouthi, V.; Sanchez-Romero, I.; Gulakova, P. E.; Minge, D.; Breithausen, B.; Schoch, S.; Janovjak, H.; Jackson, C. J.; Henneberger, C. Monitoring hippocampal glycine with the computationally designed optical sensor GlyFS. *Nat. Chem. Biol.* **2018**, *14* (9), 861−869.
(31) Lee, J. M.; Park, H. K.; Jung, Y.; Kim, J. K.; Jung, S. O.; Chung, B. H. Direct Immobilization of Protein G Variants with Various Numbers of Cysteine Residues on a Gold Surface. *Anal. Chem.* **2007**, *79* (7), 2680−2687.
(32) Couto, R. A. S.; Lima, J. L. F. C.; Quinaz, M. B. Recent developments, characteristics and potential applications of screen-printed electrodes in pharmaceutical and biological analysis. *Talanta* **2016**, *146*, 801−814.
(33) Murugappan, K.; Lee, J.; Silvester, D. S. Comparative study of screen printed electrodes for ammonia gas sensing in ionic liquids. *Electrochem. Commun.* **2011**, *13* (12), 1435−1438.
(34) Compton, R. G.; Craig, E.*Understanding Voltammetry*; World Scientific Book, 2010.
(35) Murugappan, K.; Silvester, D. S. Sensors for Highly Toxic Gases: Methylamine and Hydrogen Chloride Detection at Low Concentrations in an Ionic Liquid on Pt Screen Printed Electrodes. *Sensors* **2015**, *15* (10), 26866−26876.
(36) Algov, I.; Alfonta, L. Use of Protein Engineering to Elucidate Electron Transfer Pathways between Proteins and Electrodes. *ACS Measurement Science Au* **2022**, *2* (2), 78−90.
(37) Frew, J. E.; Hill, H. A. O. Direct and indirect electron transfer between electrodes and redox proteins. *Eur. J. Biochem.* **1988**, *172* (2), 261−269.
(38) Mitchell, J. A.; Zhang, W. H.; Herde, M. K.; Henneberger, C.; Janovjak, H.; O'Mara, M. L.; Jackson, C. J.Method for Developing Optical Sensors Using a Synthetic Dye-Fluorescent Protein FRET Pair and Computational Modeling and Assessment. In *Synthetic Protein Switches: Methods and Protocols*; Stein, V., Ed.; Springer: NY, 2017; pp 89−99.
(39) Chen, C. R.; Makhatadze, G. I. ProteinVolume: calculating molecular van der Waals and void volumes in proteins. *BMC Bioinformatics* **2015**, *16* (1), 101.
(40) Marrink, S. J.; Risselada, H. J.; Yefimov, S.; Tieleman, D. P.; de Vries, A. H. The MARTINI Force Field: Coarse Grained Model for Biomolecular Simulations. *J. Phys. Chem. B* **2007**, *111* (27), 7812−7824.
(41) Okumoto, S.; Looger, L. L.; Micheva, K. D.; Reimer, R. J.; Smith, S. J.; Frommer, W. B. Detection of glutamate release from neurons by genetically encoded surface-displayed FRET nanosensors. *P Natl. Acad. Sci. USA* **2005**, *102* (24), 8740.
(42) Fehr, M.; Frommer, W. B.; Lalonde, S. Visualization of maltose uptake in living yeast cells by fluorescent nanosensors. *Proc. Natl. Acad. Sci. U. S. A.* **2002**, *99* (15), 9846.
(43) Fehr, M.; Lalonde, S.; Lager, I.; Wolff, M. W.; Frommer, W. B. In Vivo Imaging of the Dynamics of Glucose Uptake in the Cytosol of COS-7 Cells by Fluorescent Nanosensors. *J. Biol. Chem.* **2003**, *278* (21), 19127−19133.
(44) Lager, I.; Fehr, M.; Frommer, W. B.; Lalonde, S. Development of a fluorescent nanosensor for ribose. *Febs Lett.* **2003**, *553* (1−2), 85−89.
(45) Qian, Y.; Cosio, D. M. O.; Piatkevich, K. D.; Aufmkolk, S.; Su, W.-C.; Celiker, O. T.; Schohl, A.; Murdock, M. H.; Aggarwal, A.; Chang, Y.-F.; Wiseman, P. W.; Ruthazer, E. S.; Boyden, E. S.; Campbell, R. E. Improved genetically encoded near-infrared fluorescent calcium ion indicators for in vivo imaging. *PLOS Biology* **2020**, *18* (11), e3000965.
(46) Zarowny, L.; Aggarwal, A.; Rutten, V. M. S.; Kolb, I.; Patel, R.; Huang, H.-Y.; Chang, Y.-F.; Phan, T.; Kanyo, R.; Ahrens, M. B.; Allison, W. T.; Podgorski, K.; Campbell, R. E. Bright and High-Performance Genetically Encoded Ca2+ Indicator Based on mNeonGreen Fluorescent Protein. *ACS Sensors* **2020**, *5* (7), 1959−1968.
(47) Armbruster, D. A.; Pry, T. Limit of blank, limit of detection and limit of quantitation. *Clin. Biochem. Rev.* **2008**, *Suppl 1* (Suppl 1), S49−S52.
(48) *The PyMOL Molecular Graphics System*, ver. 2.3. Schrodinger, LLC., 2010.
(49) Magnusson, U.; Salopek-Sondi, B.; Luck, L. A.; Mowbray, S. L. X-ray Structures of the Leucine-binding Protein Illustrate Conformational Changes and the Basis of Ligand Specificity *. *J. Biol. Chem.* **2004**, *279* (10), 8747−8752.
(50) Gotthard, G.; von Stetten, D.; Clavel, D.; Noirclerc-Savoye, M.; Royant, A. Chromophore Isomer Stabilization Is Critical to the Efficient Fluorescence of Cyan Fluorescent Proteins. *Biochemistry* **2017**, *56* (49), 6418−6422.
(51) Rekas, A.; Alattia, J.-R.; Nagai, T.; Miyawaki, A.; Ikura, M. Crystal Structure of Venus, a Yellow Fluorescent Protein with Improved Maturation and Reduced Environmental Sensitivity *. *J. Biol. Chem.* **2002**, *277* (52), 50573−50578.
(52) Bekker, H.; Berendsen, H.; Dijkstra, E. J.; Achterop, S.; Drunen, R.; van der Spoel, D.; Sijbers, A.; Keegstra, H.; Reitsma, B.; Renardus, M. K. R.Gromacs: A parallel computer for molecular dynamics simulations. In *Physics Computing'92* ed.; DeGroot, R. A., Nadrchal, J., Eds.; World Scientific Publishing, 1993; pp 252−256.
(53) Wassenaar, T. A.; Pluhackova, K.; Böckmann, R. A.; Marrink, S. J.; Tieleman, D. P. Going Backward: A Flexible Geometric Approach to Reverse Transformation from Coarse Grained to Atomistic Models. *J. Chem. Theory Comput.* **2014**, *10* (2), 676−690.
(54) Humphrey, W.; Dalke, A.; Schulten, K. VMD: Visual molecular dynamics. *J. Mol. Graphics* **1996**, *14* (1), 33−38.
(55) Bakan, A.; Meireles, L. M.; Bahar, I. ProDy: Protein Dynamics Inferred from Theory and Experiments. *Bioinformatics* **2011**, *27* (11), 1575−1577.

https://doi.org/10.1021/jacsau.2c00291
JACS Au 2022, 2, 2481−2490